On the evolution of particle size distributions during the bulk synthesis of High-Impact Polystyrene using PBM: towards morphology and phase inversion prediction

J. M. Maffi[1,2], D. A. Estenoz[3,4]

[1]Department of Chemical Engineering, Instituto Tecnológico de Buenos Aires (ITBA), Av. Madero 399, C.P. C1106ACD, Buenos Aires, Argentina.

[2]Consejo Nacional de Investigaciones Científicas y Técnicas (CONICET), Argentina.

[3]Instituto de Desarrollo Tecnológico para la Industria Química, INTEC (Universidad Nacional del Litoral - CONICET), Güemes 3450, C.P. 3000, Santa Fe, Argentina.

[4]Facultad de Ingeniería Química, FIQ (Universidad Nacional del Litoral - CONICET), Santiago del Estero 2829, C.P. 3000, Santa Fe, Argentina.

Corresponding author e-mail: destenoz@santafe-conicet.gov.ar,

Abstract

The mechanism of the phase inversion (PI) process that occurs during the bulk polymerization of High Impact Polystyrene (HIPS) is studied in this article. Transmission electron micrographs (TEM) were obtained for different operating conditions, varying initiator concentration, temperature, and stirring speed from a previous work. Particle size distributions were retrieved from such micrographs, and were compared to theoretical predictions. To this end, a population balance model, coupled with a heterogeneous polymerization module, was developed. The evolution of particle growth, break-up and coalescence is discussed to assess the breakage/coalescence imbalance that is thought to

occur at the inversion point. Results indicate that a different criterion for PI seems to be needed in this system.

1. Introduction

The high-impact polystyrene (HIPS) is a heterogeneous thermoplastic produced by styrene (St) polymerization in presence of polybutadiene (PB). It consists of a polystyrene (PS) matrix with dispersed PB particles, which often contain occluded PS [1]. Depending on the rubber particle size and the number of occlusions, two typical morphologies are usually identified: a 'salami morphology' (large rubber particle with several occlusions) or a 'core-shell morphology' (relatively small rubber particle with only one large occlusion), which provide the material with improved mechanical properties [2,3].

The bulk HIPS polymerization process involves four main stages: a dissolution of the rubber, a pre-polymerization of styrene (St), a finishing polymerization, and a devolatilization. The bulk pre-polymerization is carried out with intense agitation, producing free PS and a graft copolymer (PS-g-PB). The reacting system is homogeneous only at very low conversion, since the incompatibility between the PS and the PB chains forces it to undergo a phase separation mechanism, by which a dispersed, PS-rich phase is formed at the bulk of a PB-rich continuous phase [4]. St monomer is almost evenly distributed between both phases [5]. As the polymerization proceeds, more PS is produced, forcing St to migrate from the continuous to the dispersed phase, making it grow along the reaction. Eventually, the dispersed phase volume is such that a phase inversion (PI) process takes place, where, after a co-continuous transition, the PS-rich phase becomes the continuous one [6]. The desired morphology is thus developed at this crucial stage, characterized by a sudden drop of the mixture's apparent viscosity [7].

The PI process is affected by several variables, such as phase viscosity ratio, phase volume ratio, rubber cis/trans content, stirring speed, grafting efficiency (*i.e*, the ratio of grafted to total PS), reaction temperature, solvent content, PS and PB molecular weights, etc. [8–10]. It also depends on the dynamic evolution of the dispersed phase, since only a fraction of it actually participates in the inversion process, leaving behind the rest as occluded particles. Given that the strong point of HIPS is its enhanced mechanical properties, and that these are the result of the *in-situ* morphology development during the PI stage, then the understating of this phenomenon and of the relative effect of each operating variable becomes a full Chemical Engineering challenge. The optimization of the polymerization recipes and operating conditions that provide desired material properties may be achieved by fully understanding the PI phenomenon. This holds a significant interest both from academic and industrial viewpoints. In spite of its relevance, no models are currently available to predict the moment at which PI occurs and the morphology therein developed. Some investigators have suggested simplified models to explain the process of morphology development [11–13], but they do not account for the fluid-dynamic character of the phenomenon. Additionally, a few PI point correlations in polymeric systems may be found, but essentially for blends in extrusion processes [10,14,15].

There are different mechanisms by which PI may occur, the most popular being the imbalance between the coalescence and breakage rates of the dispersed particles [16]. According to this mechanism, PI will take place when particles undergo coalescence at a much faster rate than they break up. This means that the coalescence-to-breakage ratio should tend to an infinitely large value at the onset of inversion. A mathematical tool potentially capable of reproducing such a behavior is the population balance modeling (PBM), which

has already been employed in both traditional and polymeric systems [17–21] to study particle size distributions (PSDs), but not as a tool to assess a phase inversion process. On this matter, a two-region model by Hu et al. [22] predicts phase inversion curves in O/W systems assuming the coalescence vs breakage imbalance. Regarding the PI point in HIPS, some researchers have analyzed the evolution of particles before [9] and after [6,23] the inversion point, but from an experimental viewpoint.

In this work, the aforementioned mechanism is tested, in the context of the bulk polymerization of HIPS, by developing a mathematical model consisting of two modules: a heterogeneous polymerization unit and a population balance module. This model reproduces the PSD of the vitreous dispersed phase along the reaction up to the phase inversion point. It computes the growth, coalescence and breakage rates of each particle given the reactor operating conditions. The model is adjusted with experimental data and is used to assess the fluid dynamic mechanism of the PI occurrence.

2. Materials and methods

2.1. Experimental

The polymerization reactions performed in our previous work [24] were revisited, where a series of HIPS polymerizations were carried out in a 3.8-liter, stainless steel Parr reactor, equipped with a 3.85-inch anchor-type impeller, varying different operating conditions. Essentially, the effects of initiator concentration (benzoyl peroxide, BPO), temperature and stirring speed on the location of the PI points were studied. These reactions are summarized in **Table *1***. All of them were run with 6%wt PB supplied by Mitsubishi (UBEPOL, $M_{w,PB}$ = 610 000 g/mol, $M_{n,PB}$ = 210 000 g/mol, high *cis*).

Run #	[BPO] (%wt)	Temperature (ºC)	Agitation speed (rpm)
1	0.05	80	30
2	0.1	80	30
3	0.05	90	30
4	0.1	90	30
5	0.05	80	60
6	0.1	80	60
7	0.05	90	60
8	0.1	90	60

Table 1. Reaction recipes.

The PI occurrence was observed with viscosity measurements (at different shear rates), which reach a local minimum at the PI point. Along each reaction, samples were taken to determine monomer conversion (x, by methanol precipitation), grafting efficiency (ζ, by a solvent extraction technique), and PS average molecular weights ($M_{w,PS,}$ by size exclusion chromatography).

For this present work, samples before the phase inversion point of each reaction were analyzed by scanning transmission electron microscopy (STEM) on a JEOL JSM-7401F at 30 kV, after preparing them with an ultramicrotome and dyed with OsO_4 vapors.

An image analysis technique was performed on these micrographs in order to obtain the particle size distributions (PSDs) of vitreous phase. Due to intrinsic constraints of the technique, styrene evaporates during sample preparation for TEM; therefore, only "unswollen" (monomer-free) images are obtained. In each image the areas of dispersed particles are computed after a filtering and an edge-detecting process. These are then transformed to particle volumes assuming spherical geometry.

2.2. Model development

2.2.1. Heterogeneous polymerization model

In order to compute the evolution of the physical properties of the polymerizing system, which depend on monomer conversion, PS molecular weights and amount of graft copolymer, a theoretical polymerization model is needed. In this case, the heterogeneous bulk polymerization of St in presence of PB was modeled similarly to Casis et al. [25], but extended to compute the evolution of a given particle's volume. The main hypotheses behind this model are the following:

1. The flux of styrene from the continuous to the dispersed phase serves to transfer the PS propagating radicals in the rubbery phase to the vitreous phase. However, copolymer molecules or copolymer propagating radicals are left in the rubber-rich phase.
2. The flux of low molar mass species (styrene, initiator) is envisaged to keep its partition coefficient as close to 1 (one) as possible.
3. Each phase follows the kinetic mechanism describe in **Table *2***, but rate constants are allowed to differ between each phase. This is especially considered for the termination rate constants, since the gel effect may vary according to the polymer concentration in each phase. This mechanism includes thermal and chemical initiation (by a monofunctional initiator), propagation, transfer to the monomer and to the rubber, and termination by combination.
4. Long chain approximation is assumed, by which styrene is mostly consumed in the propagation reactions.
5. The polymerization is considered to be heterogeneous from the moment it begins, although it may be changed easily to phase separate at any given time.

Proposed kinetic mechanism	**Nomenclature**	
Initiation	St	Monomer
$3St \xrightarrow{k_{i0}} 2S_1^\bullet$	$S_1^\bullet$	Monomer radical
$I_2 \xrightarrow{f\,k_d} 2I^\bullet$	I_2	Initiator
$I^\bullet + St \xrightarrow{k_{i1}} S_1^\bullet$	$I^\bullet$	Initiator radical
$I^\bullet + B \xrightarrow{k_{i2}} P_0^\bullet$	B	Unreacted butadiene unit
$P_0^\bullet + St \xrightarrow{k_{i3}} P_1^\bullet$	$P_0^\bullet$	Primary radical produced by attack to a butadiene unit
Propagation	$P_1^\bullet$	Copolymer radical with one styrene unit
$S_n^\bullet + St \xrightarrow{k_p} S_{n+1}^\bullet$	$P_n^\bullet$	Copolymer radical with n repetitive units of St in active branch.
$P_n^\bullet + St \xrightarrow{k_p} P_{n+1}^\bullet$	$S_n^\bullet$	Free PS radical with n repetitive units.
Transfer	S_n	PS with n repetitive units.
$S_n^\bullet + St \xrightarrow{k_{fM}} S_n + S_1^\bullet$	P_n	Copolymer with n repetitive St units.
$P_n^\bullet + St \xrightarrow{k_{fM}} P_n + S_1^\bullet$		
$P_0^\bullet + St \xrightarrow{k_{fM}} B + S_1^\bullet$		
$S_n^\bullet + B \xrightarrow{k_{fG}} S_n + P_0^\bullet$		
$S_n^\bullet + P_n \xrightarrow{k_{fG}} S_n + P_n^\bullet$		
Termination		
$S_n^\bullet + S_m^\bullet \xrightarrow{k_{tc}} S_{n+m}$		
$S_n^\bullet + P_m^\bullet \xrightarrow{k_{tc}} P_{n+m}$		
$P_n^\bullet + P_m^\bullet \xrightarrow{k_{tc}} P_{n+m}$		
$P_n^\bullet + P_0^\bullet \xrightarrow{k_{tc}} P_n$		
$S_n^\bullet + P_0^\bullet \xrightarrow{k_{tc}} P_n$		
$P_0^\bullet + P_0^\bullet \xrightarrow{k_{tc}} P_0$		

Table 2. Suggested kinetic mechanism.

One of the most important features to be calculated with this model – necessary for the population balance – is the rate of change of a given (vitreous) particle volume. Considering the mentioned hypotheses and assuming additive volumes, the evolution of the total dispersed phase volume, $\dot{V}_v$, is derived from its definition:

$$\dot{V}_v = \frac{\dot{m}_{St,v}}{\rho_{St}} + \frac{\dot{m}_{PS}}{\rho_{PS}} \tag{1}$$

where $\dot{m}_{St,v}$ and $\dot{m}_{PS}$ are the rate of change of St and PS masses respectively. Accepting the "long chain approximation", by which St is mainly consumed by propagation reactions, these rates of change are calculated as follows:

$$\dot{m}_{St,v} = -k_{pv}[St_v][S_v^\bullet]V_v M_{St} + \dot{F} \tag{2}$$

$$\dot{m}_{PS} = k_{pv}[St_v][S_v^\bullet]V_v M_{St} + k_{pr}[St_r]([S_r^\bullet] + [P^\bullet])V_r M_{St} \tag{3}$$

where $\dot{F}$ is the flux of transferred styrene from the continuous to the dispersed phase. Subscripts *v* and *r* stand for vitreous and rubbery phase respectively.

The St consumption in the rubber-rich phase is:

$$\dot{m}_{St,r} = -k_{pr}[St_r]([S_r^\bullet] + [P^\bullet])V_r M_{St} - \dot{F} \tag{4}$$

In turn, $\dot{F}$ is calculated so that the St partition coefficient between each phase is satisfied at all times:

$$[St_v] = [St_r] \tag{5}$$

$$m_{St,v}\left(\frac{m_{PB}}{\rho_{PB}} + \frac{m_{St,r}}{\rho_{St}}\right) = m_{St,r}\left(\frac{m_{PS}}{\rho_{PS}} + \frac{m_{St,v}}{\rho_{St}}\right) \tag{6}$$

Expanding and differentiating:

$$\dot{m}_{St,v}\frac{m_{PB}}{\rho_{PB}} = \dot{m}_{St,r}\frac{m_{PS}}{\rho_{PS}} + m_{St,r}\frac{\dot{m}_{PS}}{\rho_{St}} \tag{7}$$

Using Eqs. (2)-(4):

$$\left(\dot{F} - Rp_v M_{St} V_v\right)m_{PB}\frac{\rho_{PS}}{\rho_{PB}} = -\left(\dot{F} + Rp_r M_{St} V_r\right)m_{PS} + m_{St,r}(Rp_v V_v + Rp_r V_r)M_{St} \tag{8}$$

from which:

$$\dot{F} = \frac{\left(m_{St,r} + m_{PB}\right) Rp_v V_v + \left(m_{St,r} - m_{PS}\right) Rp_r V_r}{m_{PB} \frac{\rho_{PS}}{\rho_{PB}} + m_{PS}} M_{St} \tag{9}$$

where Rp_v and Rp_r are the polymerization rates in the vitreous and rubbery phases respectively. Using the vitreous phase volume fraction, which depends only on monomer conversion:

$$\dot{F} = \frac{\left(m_{St,r} + m_{PB}\right) Rp_v + \left(m_{St,r} - m_{PS}\right) Rp_r \frac{(1-\phi_v)}{\phi_v}}{m_{PB} \frac{\rho_{PS}}{\rho_{PB}} + m_{PS}} M_{St} V_v \tag{10}$$

Finally, the flux of monomer that is received by one droplet of volume v, $\dot{F}_{(v)}$, is simply Eq. (10) evaluated at $V_v = v$:

$$\dot{F}_{(v)} = \dot{F} \frac{v}{V_v} \tag{11}$$

Therefore, the rate at which the volume of a given particle changes over time is:

$$\dot{V}_{(v)} = \left[k_{pv} [St_v] [S_v^{\bullet}] \left(\frac{1}{\rho_{PS}} - \frac{1}{\rho_{St}} \right) M_{St} + \frac{\dot{F}}{\rho_{St} V_v} \right] v \tag{12}$$

Note that the term in square brackets is solely a function of time. The remaining equations of the polymerization module are described in the Appendix, where a more detailed balance for each radical species is described.

2.1.2. Population balance model – PSD prediction

The population balance equation (PBE) is the partial differential equation describing the evolution of the number density function of vitreous droplets of volume v per unit of physical volume at time t, $f_{(v,t)}$. Considering binary break-up and only two-particle coalescence in a

perfectly mixed tank – and neglecting Ostwald ripening due to low diffusivity of the dispersed phase [26,27] – this equation reads:

$$\frac{\partial f_{(v,t)}}{\partial t} + \frac{\partial}{\partial v}\left(\dot{V}_{(v,t)} f_{(v,t)}\right) = 2\int_{v}^{\infty} \omega_{b(v')} f_{(v',t)} \beta_{(v|v')} dv' - \omega_{b(v)} f_{(v,t)} + \frac{1}{2}\int_{0}^{\infty} \omega_{c(v-v',v')} f_{(v-v',t)} f_{(v',t)} dv' - f_{(v,t)} \int_{0}^{\infty} \omega_{c(v,v')} f_{(v',t)} dv' \quad (13)$$

where $\dot{V}_{(v,t)}$ is the rate of change of a particle's volume (calculated with Eq. (12)), $\omega_{b(v)}$ is the fractional break-up frequency of particles of volume v, $\beta_{(v|v')}$ is the probability density function of a particle of volume v being born after breakage of a particle of volume v', and $\omega_{c(v,v')}$ is the average coalescence frequency of particle pairs of volumes v and v'. The latter is usually expressed in the form of the product between a collision frequency, $\omega_{cd(v,v')}$, and a coalescence efficiency, $\lambda_{(v,v')}$.

A large number of expressions for ω_b, β, ω_{cd} and λ are available in literature [20,28–30], usually developed for O/W dispersions, but also used in polymeric systems since the physics behind them do not differ considerably [31–33]. None have yet been used in the bulk polymerization of HIPS, but some can be found in other polymeric systems [17,21]. In this case, the selected functions were chosen after reviewing their field application and similarity to the system of interest in this work. As a general rule, expressions developed for bubbles in liquids are disregarded. The chosen kernels are the following [34–37]:

$$\omega_{b(v)} = C_{1b}\varepsilon^{1/3}\,\mathrm{erfc}\left(\sqrt{C_{2b}\frac{\gamma}{\rho_c\varepsilon^{2/3}}\left(\frac{\pi}{6v}\right)^{5/9} + C_{3b}\frac{\eta_d}{\sqrt{\rho_c\rho_d}\varepsilon^{1/3}}\left(\frac{\pi}{6v}\right)^{4/9}}\right) \tag{14}$$

$$\beta_{(v|v')} = 30\left(\frac{v}{v'}\right)^2\left(1-\frac{v}{v'}\right)^2 \tag{15}$$

$$\omega_{cd(v,v')} = C_{1c}h_{(v,v')}\frac{\varepsilon^{1/3}}{1+\phi_d}\left(v^{2/9}+v'^{2/9}\right)^{1/2} \tag{16}$$

$$\lambda_{(v,v')} = \lambda_1 + \lambda_2 - \lambda_1\lambda_2 \tag{17}$$

where subscripts *c* and *d* refer to the continuous and the dispersed phase respectively, η is the apparent viscosity, ε is the mean energy dissipation rate and ϕ_d is the dispersed phase volume fraction. The factor $h_{(v,v')}$ is a radial distribution function that accounts for the fact that the probability of a given particle to "see" another is not uniform when the dispersion is dense (high dispersed fraction). In this work, the one developed by Song et al. [38] (based on the Carnhan-Starling equation of state) is used:

$$h_{(v,v')} = \frac{1}{1-\phi_d} + \frac{3}{2(1-\phi_d)^2}\xi_{(v,v')} + \frac{1}{(1-\phi_d)^3}\xi_{(v,v')}^2 \tag{18}$$

with

$$\xi_{(v,v')} = 2\left(\frac{vv'}{v+v'}\right)^{1/3}\sum_{i=1}^{N}\widehat{N}_i v_i^{2/3} \tag{19}$$

where $\widehat{N}_i$ is the number of particles of size v_i per unit volume of physical space and *N* is the total number of particles.

In turn, the terms in the equation for the coalescence efficiency are:

$$\lambda_{1(v,v')} = \exp\left[-C_{2c}\frac{\eta_c\rho_c\varepsilon}{\gamma^2}\left(\frac{v^{1/3}v'^{1/3}}{v^{1/3}+v'^{1/3}}\right)^4\right] \tag{20}$$

$$\lambda_{2(v,v')} = \exp\left[-C_{3c}\frac{\gamma}{\rho_d\varepsilon^{2/3}}\frac{(v+v')}{vv'}\frac{\left(v^{2/3}+v'^{2/3}\right)}{(v^{2/9}+v'^{2/9})}\right] \tag{21}$$

Eq. (13) is to be supplied with initial and boundary conditions before it is solved. In this case, the following assumptions are considered: i) nucleation is negligible, ii) there are no particles of a sufficiently large mass, and iii) initial particle size distributions are $\sim\mathcal{LN}(\mu,\sigma)$ with respect to particle diameter, a fact that has been extensively verified for many liquid-liquid dispersions [39–41]. In terms of particle volume, these assumptions yield the following initial and boundary conditions, considering spherical geometry:

$$\begin{cases} \dot{V}_{(v_{min},t)}f_{(v_{min},t)} = 0 \\ f_{(v_{max},t)} = 0 \\ f_{(v,0)} = \dfrac{\widehat{N}_0}{3v\sigma\sqrt{2\pi}}\exp\left\{-\dfrac{\left[\ln(6v/\pi)^{1/3}-\mu\right]^2}{2\sigma^2}\right\} \end{cases} \tag{22}$$

where $\widehat{N}_0$ is the number of initial particles per unit volume of reacting mixture.

In the implementation of the PBE, time is discretized in the same intervals as the polymerization module (for consistency) and particle volume is discretized in a logarithmically spaced grid (to cover a wide range of particle sizes). A moving pivot technique by Kumar and Ramkrishna is used to solve the PBE [42,43], whose discretized form is the following:

$$\frac{d\widehat{N}_{i(t)}}{dt} = 2\sum_{j=1}^{NI} \omega_{b(u_j)}\widehat{N}_{j(t)}\left[\int_{u_{i-1}}^{u_i} \frac{v-u_{i-1}}{u_i-u_{i-1}}\beta_{(v,u_j)}\,dv + \int_{u_i}^{u_{i+1}} \frac{u_{i+1}-v}{u_{i+1}-u_i}\beta_{(v,u_j)}\right]$$
$$- \omega_{b(u_j)}\widehat{N}_{j(t)}$$
$$+ \sum_{u_{i-1}\le u_j+u_k\le u_{i+1}}^{i\ge j\ge k} \left(1-\frac{1}{2}\delta_{(u_j-u_k)}\right)\nu\omega_{c(u_j,u_k)}\widehat{N}_{j(t)}\widehat{N}_{k(t)} \quad (23)$$
$$- \widehat{N}_{i(t)}\sum_{j=1}^{NI} \omega_{c(u_i,u_j)}\widehat{N}_{j(t)}$$

where $\delta_{(u)}$ is the Dirac delta function, here used to avoid computing repeated pairs of particles that yield the same result, and ν is an allocation function to account for the fact that not all particles are born in the discretized pivots and must therefore be distributed in a way that both number and mass are preserved:

$$\nu = \begin{cases} \dfrac{u_j+u_k-u_{i-1}}{u_i-u_{i-1}} \\ \dfrac{u_{i+1}-(u_j+u_k)}{u_{i+1}-u_i} \end{cases} \quad (24)$$

2.1.3. Phase properties

The density of St, PS and PB and the viscosities of each phase are calculated with the expressions found in **Table *3***. Since the mixture exhibits non-Newtonian behavior (as analyzed in our previous work), it is necessary to compute the shear rate at reaction conditions. For anchor-type impellers, the following expression applies [44]:

$$\dot{\gamma} = 25n\sqrt{\frac{D_I}{D_T}} \tag{25}$$

where n is the stirring speed, D_I is the impeller diameter and D_T that of the reactor.

In turn, interfacial tension (γ) is computed with an expression by Kwok and Neumann [45] for a copolymer-free system, γ_0, and a correction by Noolandi and Hong [46] to account for its reduction in the presence of the generated graft copolymer, $\Delta\gamma$:

$$\gamma_0 = \sigma_v + \sigma_r - 2\sqrt{\sigma_v\sigma_r}\exp[-\alpha(\sigma_v - \sigma_r)^2] \tag{26}$$

$$\Delta\gamma = W\phi_{cop}\left\{\frac{\chi}{2}(\phi_{PB} + \phi_{PS}) + \frac{1}{z_{St} + z_B}\left[1 - \exp\left[\frac{\chi}{2}(z_{St} + z_B)(\phi_{PB} + \phi_{PS})\right]\right]\right\} \tag{27}$$

where χ is the Flory-Huggins parameter for PS-PB (calculated with solubility parameters [47]), and z_{St} and z_B are the polymerization degrees of PS and PB in a copolymer whose volume fraction is ϕ_{cop}. In turn, α is a universal constant of value 1.247 10^{-3} m^2/mN^2 and W is the width at half height of the copolymer profile, here approximated to [48]:

$$W = b\left[\frac{2\chi}{3(1 - \phi_{St})}\right]^{0.5} \tag{28}$$

with b being the average Kuhn length (6.95 Å [49]).

The surface tension of the vitreous phase, σ_v, is computed with the correlation obtained from the experimental data published by Cerpa-Gallegos et al. [50]:

$$\sigma_v = S_0 + K\left(1 - w_{St,v}\right)^a M_{w,PS}^b \tag{29}$$

where S_0 = 31.627 mN/m, K = 2.75 mN/m, a = 1.07725 and b = 0.49657. The PS weight-average molecular weight is here expressed in kg/mol.

The surface tension of the rubbery phase, σ_r, is calculated with the mixing rule by Prigogine and Marechal [51]:

$$\sigma_r = S_0\phi_{St,r} + \sigma_{PB}\left(1 - \phi_{St,r}\right) \tag{30}$$

where σ_{PB} is the surface tension of PB, here calculated with the Parachor method using the group contributions by Sugden [52], and $\phi_{St,r}$ is the volume fraction of styrene in the rubber-rich phase.

Finally, the temperature dependence is computed using the ratio of the phase densities [53]:

$$\sigma_{i(T)} = \sigma_{i(T_0)}\left(\frac{\rho_{i(T)}}{\rho_{i(T_0)}}\right)^4 \tag{31}$$

Densities (kg/m^3, T in ^{o}C)	Reference
$\rho_{St} = 924 - 0.918T$	[54]
$\rho_{PS} = 1084.8 - 0.605T$	[54]
$\rho_{PS} = [1.097 \times 10^{-3} + 7.679 \times 10^{-7}T - 2.222 \times 10^{10}T^2]^{-1}$	[55]
Viscosities (cP, T in ^{o}K, $M_{w,PS}$ in g/mol)	
$\eta_r = \exp\left[1052.19\left(\frac{1}{T} - \frac{1}{298}\right) + \ln(\eta_{r0})\right]$	[56]
$\ln(\eta_{r0}) = 38.7[1 - \exp(-1.6974\dot{\gamma})]\left(1 - w_{St,r}\right) + \frac{2.4589}{\dot{\gamma} + 0.3472}$	[57]
$\eta_v = \frac{\eta_{0v}}{\left(1 + \frac{\eta_{0v}}{35000}\right)^{0.6}}$	[58]

$$\eta_{0v} = 1000 \exp\left\{-11.091 + \frac{1109}{T} + {M_{w,PS}}^{0.1413}\left[12.032 w_{PS,v} - 19.501 {w_{PS,v}}^2 + 2.923 {w_{PS,v}}^3 + \frac{1}{T}\left(-1327 w_{PS,v} + 1359 {w_{PS,v}}^2 + 3597 {w_{PS,v}}^3\right)\right]\right\} \quad [58]$$

Table 3. Correlations for densities and viscosities used in this work.

3. Results

Figure *1* shows TEM micrographs for selected samples before the PI point. Subfigures a)-c) are taken around the same monomer conversion, and somewhat larger domains are observed in the latter. This corresponds to reaction 6 (80ºC, 0.1% BPO, 60 rpm), which was run at a higher stirring speed than reaction 2 (80ºC, 0.1% BPO, 30 rpm), whose micrograph corresponds to subfigure a). Reaction 3, which was conducted at a higher temperature, but at a lower initiator concentration (90ºC, 0.05% BPO, 30 rpm) yielded similar particle sizes, which may imply that the opposed effects that these variables exert on interfacial tension were balanced out, at least at this conversion level. It should be noted that this effect may change considerably along the reaction and affect coalescence efficiency substantially, enough to trigger PI at an early stage, as discussed in our previous work [24].

In turn, the large domains observed in subfigure d), corresponding to reaction 8 at almost 15% conversion, are in agreement with the fact that the system is near the onset of inversion.

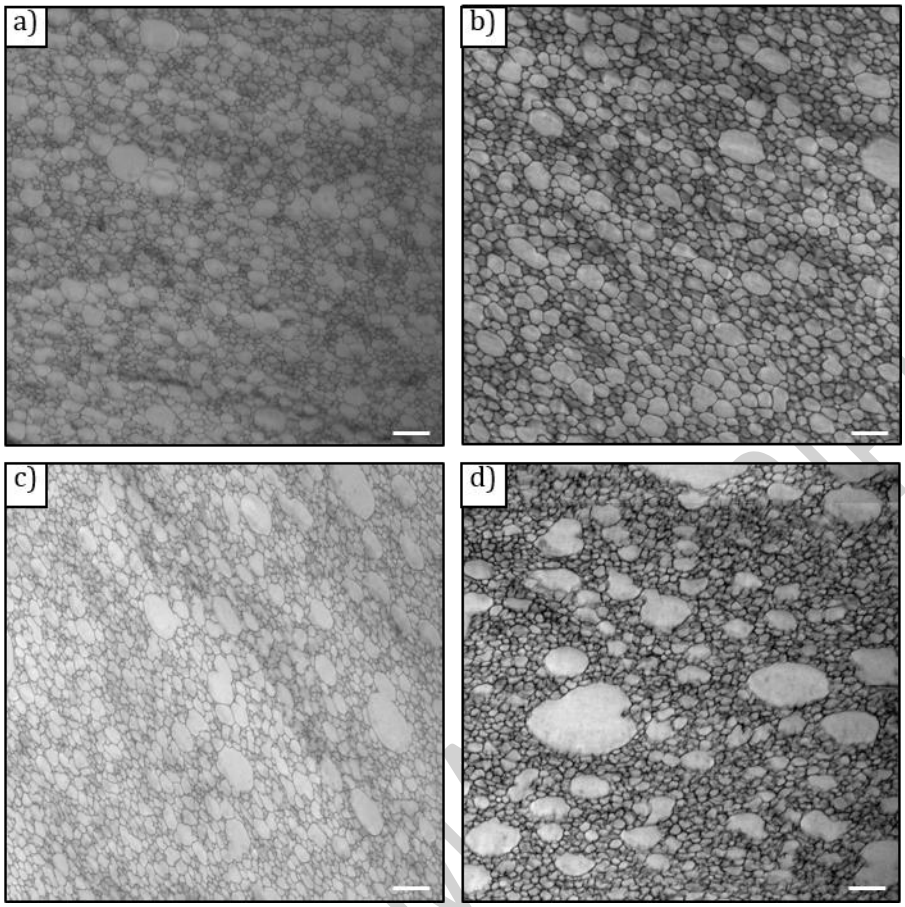

Figure 1. TEM micrographs for selected samples a) reaction 2, 9.86% conversion, b) reaction 3, 8.22%, c) reaction 6, 9.52%, d) reaction 8, 14.66%. Scale bar is 2 μm.

Regarding the simulation results, the kinetic heterogeneous polymerization module is solved in the first place, with a traditional 2nd order Rosenbrock formula, suitable for stiff systems. In this case, kinetic parameters are taken from literature [59–61] and a very good agreement with the experimental observations is observed, as shown in **Figure *2***. Given the error by excess produced in the determination of the grafting efficiency [59], it is expected that the experimental points lie somewhat above the predicted results.

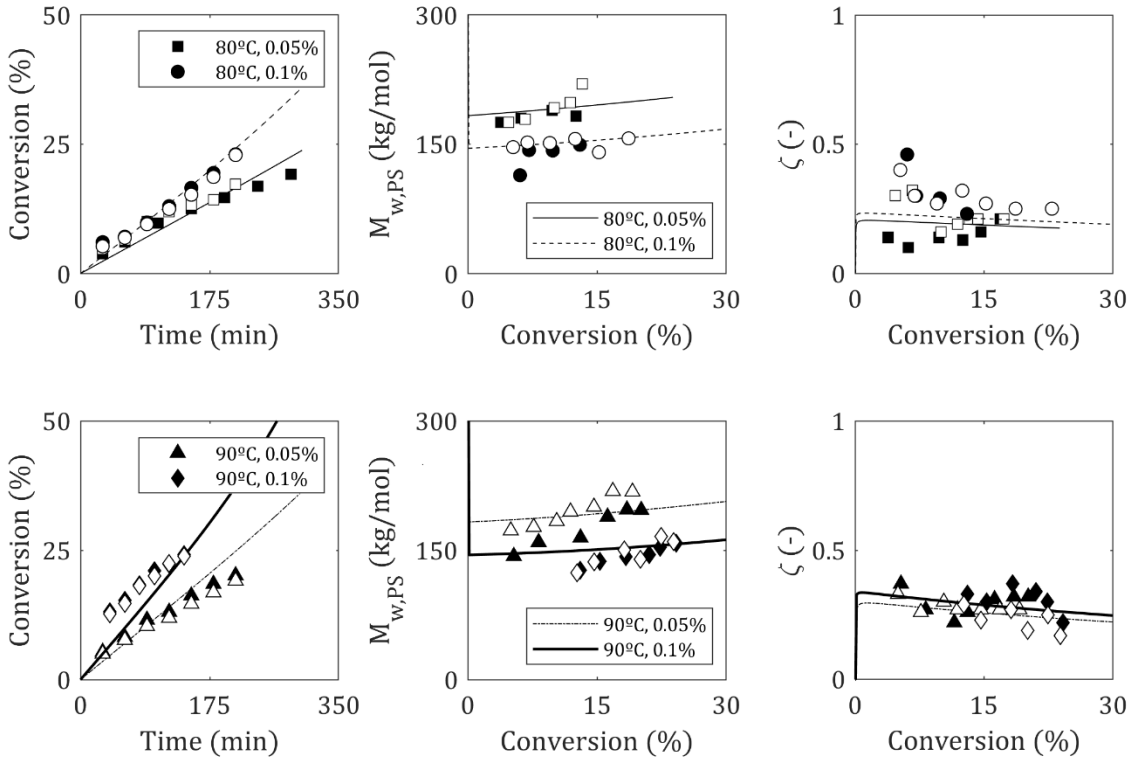

Figure 2. Evolution of conversion, PS molecular weight and grafting efficiency as measured experimentally and predicted by the polymerization model. Black markers refer to reactions at 30 rpm, and white markers, at 60 rpm.

The evolution with time of the main reaction variables (conversion, molecular weights, copolymer concentration, grafting efficiency, *etc.*) are used to calculate the physical properties along the reaction, as well as the growth rate of the dispersed phase (Eq. (12)). These are then fed to the PBE model, which calculates the PSD of the vitreous phase along the polymerization. The adjusting procedure consists of finding an acceptable order of magnitude for the values of C_{1b}, C_{2b}, C_{3b}, C_{1c}, C_{2c} and C_{3c}, and then fine-tuning with μ and σ for each reaction. While it is expected that reaction conditions (temperature, initiator concentration and stirring speed) affect the initial PSD (as per phase separation theory

[62,63]), these effects are not known due to the lack of experimental evidence. Then, these parameters are adjusted as part of the fitting procedure.

Figure *3* shows the PSDs as obtained from the selected TEM images (only a few are shown, to avoid redundancy) of samples taken before the PI point. These are compared with the predicted curves by the PBE model, resulting in a very good agreement.

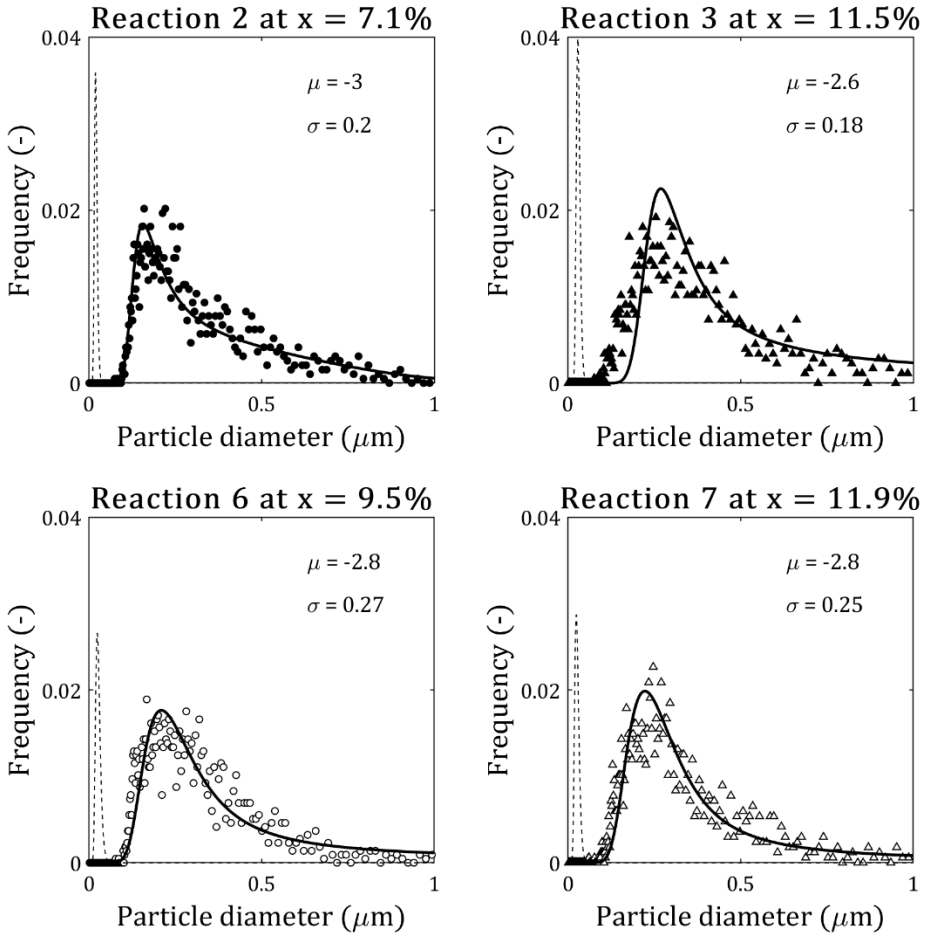

Figure 3. Particle size distributions of selected TEM images. Dashed lines correspond to the initial PSD. Each subfigure shows the values of μ and σ used for the initial conditions.

The values of the adjusted parameters for the PBE model are shown in **Table *4***, while kinetic parameters for the polymerization module are displayed in **Table *5***.

Parameter	Value
C_{1b}	10^{-4}
C_{2b}	10^{-5}
C_{3b}	10^{-5}
C_{1c}	$5 \cdot 10^{-4}$
C_{2c}	10^{3}
C_{3c}	10^{-9}

Table 4. Values of the adjusted parameters.

Parameter	Unit	Value	Reference
k_d	1/s	$2.97 \cdot 10^{15}\ e^{-16179/T}$	[64]
k_{i0}	$L^2/(mol^2 \cdot s^2)$	$2.3 \cdot 10^{6}\ e^{-15005/T}$	[65]
k_{i1}	L/(mol·s)	$8.37 \cdot 10^{5}\ e^{-2650/T}$	[59]
k_{i2}	L/(mol·s)	$5.27 \cdot 10^{5}\ e^{-2650/T}$	[59]
k_{i3}	L/(mol·s)	$2.16 \cdot 10^{7}\ e^{-3905/T}$	[66]
k_p	L/(mol·s)	$2.16 \cdot 10^{7}\ e^{-3905/T}$	[66]
k_{fM}	L/(mol·s)	$7.81 \cdot 10^{6}\ e^{-6435/T}$	[59]
k_{fG}	L/(mol·s)	$1.11 \cdot 10^{10}\ e^{-8898/T}$	[59]
k_{tc}	L/(mol·s)	$1.66 \cdot 10^{9}\ e^{-[843/T+2(C_1 x+C_2 x^2+C_3 x^3)]}$	[60]
f	-	0.9	Adjusted in this work

Table 5. Values of the kinetic parameters used in the polymerization module. C_1 = 2.57 - 0.00505T, C_2 = 956 - 0.01767T, C_3 = -3.03 + 0.00785T. x stands for polymer weight fraction.

3.1. Phase inversion criterion

Based on the location of the viscosity local minimax points, the phase inversion periods were established for each reaction in our earlier work, and are here reproduced in **Table *6*** for convenience.

T	[BPO]	Stirring speed (rpm)	
ºC	%wt	30	60
80	0.05	12 – 15 %	10 – 14 %
	0.1	13 – 17 %	15 – 18 %
90	0.05	10 – 12 %	10 – 12 %
	0.1	15 – 18 %	15 – 18 %

Table 6. Phase inversion periods for each reaction.

The evolution of total particle break-up (Ω_b) and coalescence (Ω_c) frequencies may then be observed throughout the reaction, with special attention to the PI periods highlighted in **Table *6***. These are calculated with the PBE model as follows:

$$\Omega_{b(T)} = V_{T(t)} \int_0^\infty \omega_{b(v)} f_{(v,t)} dv \tag{32}$$

$$\Omega_{c(t)} = V_{T(t)} \int_0^\infty f_{(v,t)} \int_0^\infty \omega_{c(v,v')} f_{(v',t)} dv' dv \tag{33}$$

Where V_T is the total volume of the polymerizing system. Note that Ω_c is the number of particle *pairs* coalescing per unit time.

If the widely accepted mechanism for PI occurrence applies in this case, then a sharp increase in the evolution of $\Omega_{c(t)}$ should be observed at some point during the reaction. **Figure *4*** shows, however, that this is not the case.

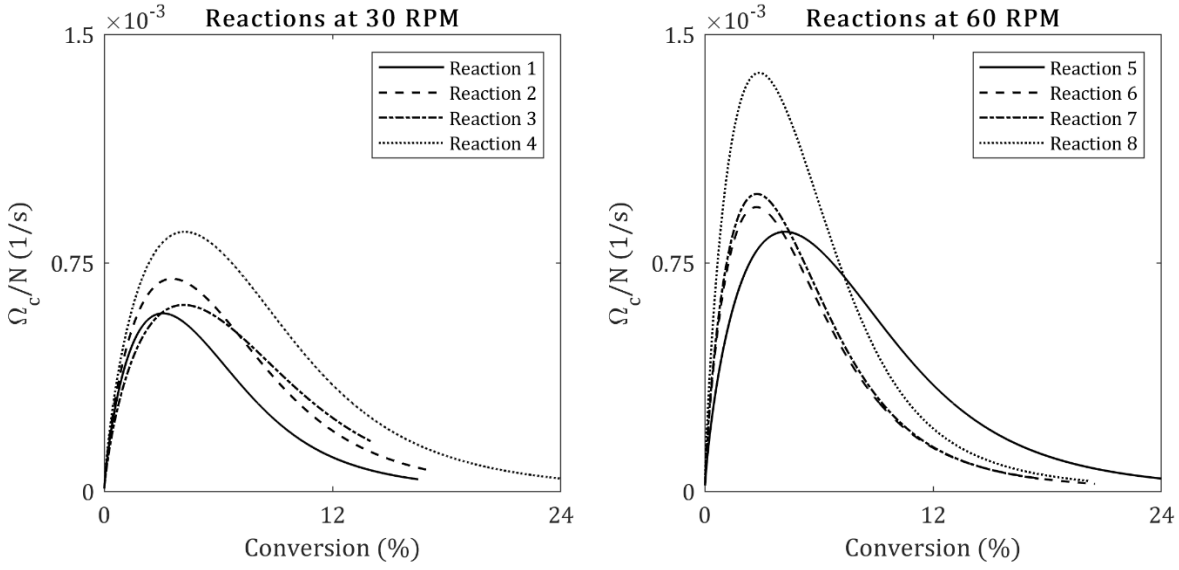

Figure 4. Fraction of particle pairs coalescing per unit time as calculated by the PBE model.

As observed, no exponential increase is observed in any case. On the contrary, coalescence rates tend to decrease after an early increase in the reaction (which is expected since a large number of small particles are found at the initial stage, and coalescence of small particles is highly effective [67]). This evolution implies that, as the reaction proceeds, less and less particles actually participate in the coalescence process. Some authors argue that what should increase acutely is the coalescence-to-breakage ratio [68], since breakage should be ineffective around the PI point. Notwithstanding, this is not observed in any reaction either, as shown in **Figure *5***.

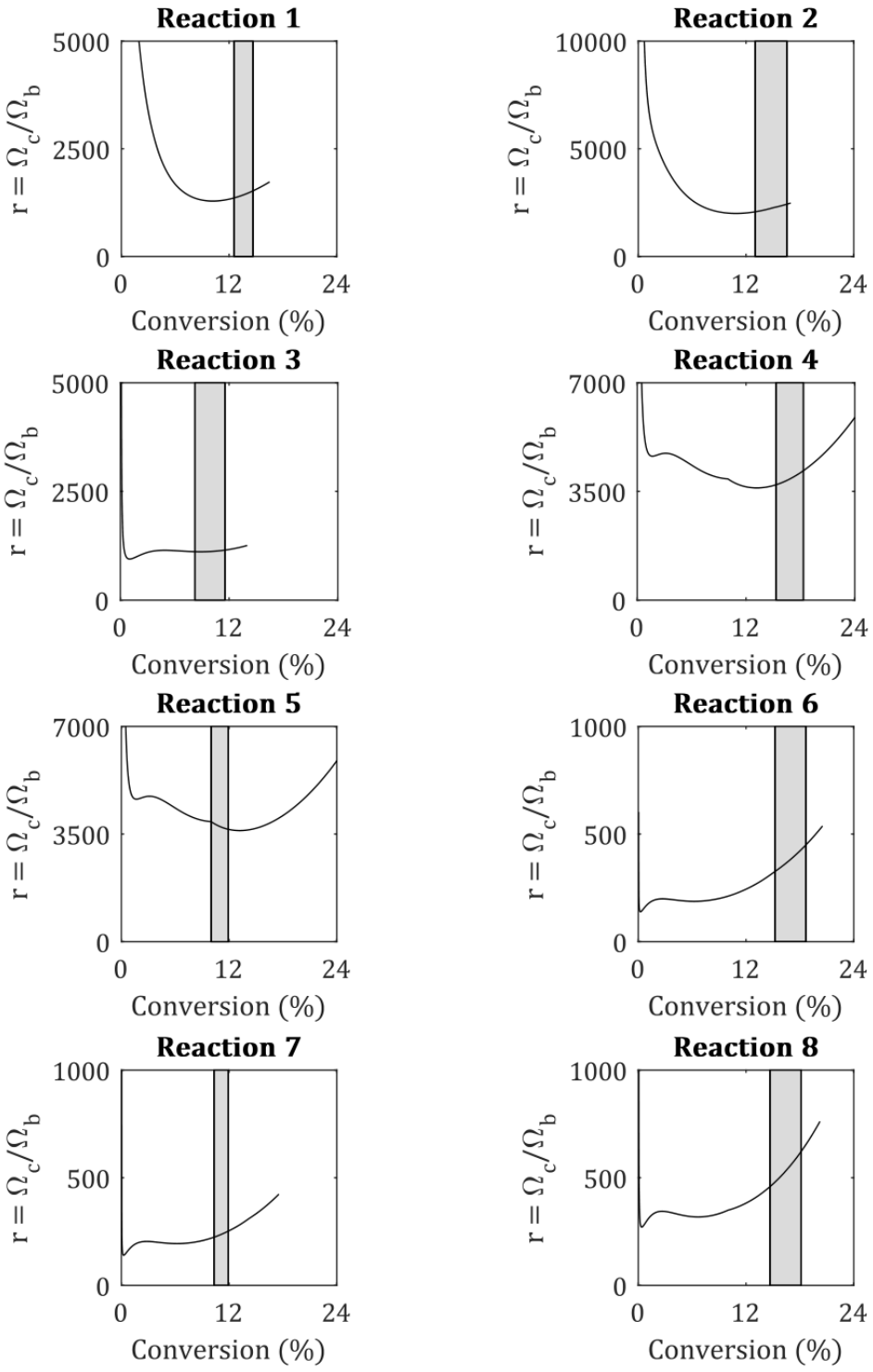

Figure 5. Coalescence-to-breakage ratio as predicted by the PBE model. The PI zones are highlighted in gray as a visual aid.

4. Discussion

Results shown so far seem to indicate that the criterion frequently cited for PI may not apply in this system. In traditional O/W experiments aiming to study catastrophic phase inversion, the set of liquids is always the same (these do not vary during the addition of dispersed phase). This is clearly not the case in a reacting system, especially in a one where viscosities and interfacial tension may vary substantially. It may be reasonable, then, that PI criteria could vary between such systems.

A more detailed physical analysis shows that the following is observed along the reaction:

1. Phase viscosities increase significantly.
2. Dispersed phase density increases.
3. Interfacial tension increases (due to monomer loss) but is attenuated by the presence of graft copolymer.
4. The net number of particles decreases along the reaction ($\Omega_c > \Omega_b$ according to **Figure *5***).

These observations point towards a natural *decrease* in the collision frequency (and thus, in the coalescence rate) along the reaction. Consequently, the predicted evolutions in **Figure *4*** would appear qualitatively reasonable. The necessary condition that allows PI to occur is that $\Omega_c > \Omega_b$, which is shown to be the case in these reactions. Naturally, if the breakage rate was higher than the coalescence rate, no PI could ever occur as more, smaller particles would be formed, producing a finer emulsion instead of a continuous matrix.

In this system, phase inversion does not occur abruptly, as is the case in may O/W dispersions [69–71]. Rather, this process happens through a transitional co-continuous arrangement

before reaching the inverted configuration. In that sense, low coalescence frequencies (as the ones predicted by the PBE model) would be in agreement with such a behavior. In consequence, predicting the PI point by an abrupt increase in the coalescence rate (or the coalescence-to-breakage ratio) seems not to apply in this case.

The physics predicted by the PBE model may be further assessed if the location of the PI points are known beforehand. This is described in what follows.

A differential timestep before the inversion point, when the morphology is essentially developed, there will be a fraction Φ of vitreous phase that will become the continuous one, leaving a fraction $1-\Phi$ as occlusions. A qualitative representation of this situation is described in **Figure *6***. If this is the case, the cumulative frequency (in particle volume) should increase smoothly up to the point where it accumulates a fraction $1-\Phi$ of dispersed phase and then increase abruptly to 1.

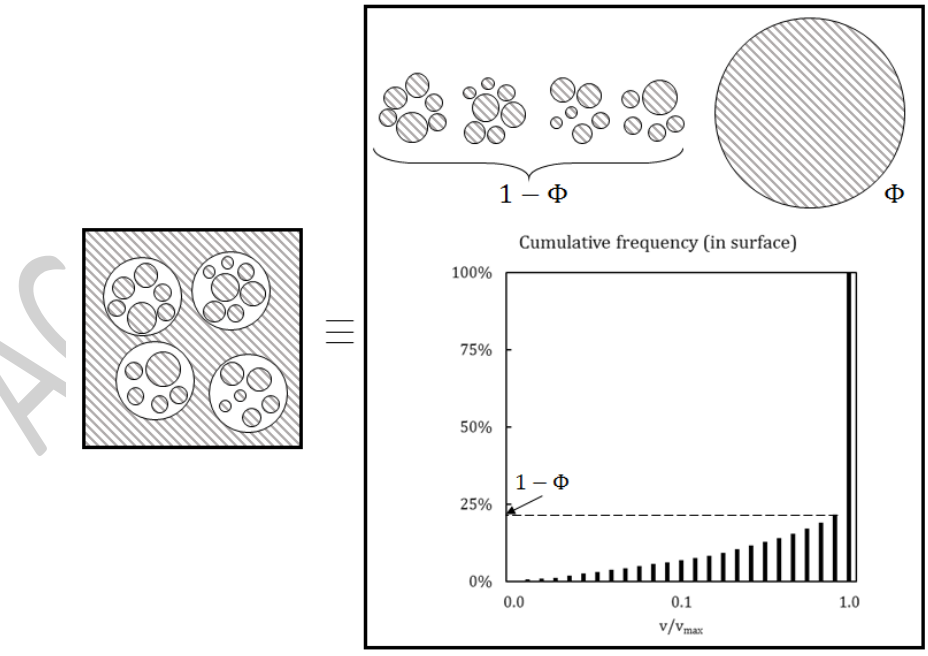

Figure 6. Visual representation of the particle cumulative frequency at the PI point.

The PBE model should be able to reproduce the continuous equivalent of the discrete cumulative frequency shown in **Figure *6***, and its sharp increase should be detectable with its derivative. If the fraction of occluded phase at the PI point, ϕ_{oc}, is known, it may be used to analyze if the location of the spike in the cumulative frequency derivative occurs around such a point. Under the hypothesis that occlusions do not escape from the dispersed phase between the PI point and the time at which the sample is taken, the occluded phase fraction observed by TEM may be used to calculate the value of Φ, as follows:

$$\phi_v = \frac{V_{v,c} + V_{v,oc}}{V_T} = \frac{V_{v,c} + V_r \dfrac{\phi_{oc}}{1-\phi_{oc}}}{V_T} \tag{34}$$

where $V_{v,c}$ is the volume of vitreous phase that constitutes the continuous matrix and $V_{v,oc}$ the volume of vitreous phase that is left behind as occlusions. This expression may be evaluated at $x = x_{PI}$, the conversion at PI, and rearranged to introduce $\Phi = \frac{V_{v,c}}{V_v}$:

$$\phi_{v\,(x=x_{PI})} = \left[\phi_v \Phi + (1-\phi_v)\frac{\phi_{oc}}{1-\phi_{oc}}\right]\Bigg|_{x=x_{PI}} \tag{35}$$

from which:

$$\Phi = \left[1 - \frac{(1-\phi_v)}{1-\phi_{oc}}\frac{\phi_{oc}}{\phi_v}\right]\Bigg|_{x=x_{PI}} \tag{36}$$

From our previous work, the average occluded phase fraction around the PI points of each reaction are recovered with an image analysis technique performed on the available TEM images (reaction 4 showed poor results in terms of image quality and no calculation was

performed for this case) and are here summarized in **Table *7***, together with the corresponding value of Φ.

Reaction	ϕ_{oc}	Φ
1	0.5216	0.3692
2	0.5742	0.3059
3	0.4825	0.3196
5	0.4432	0.4368
6	0.5757	0.3782
7	0.4438	0.4186
8	0.5903	0.3215

Table 7. Average occluded phase fractions for each reaction around the PI point and the corresponding calculated inversion fraction.

The cumulative frequency distributions, φ, and its derivatives at the PI point are shown in ***Figure 7***. As observed, the peaks in the derivative curves occur around the calculated values of Φ. This means that the consistency of the PBE model is acceptable; it may potentially be used to predict the morphology that is developed at the PI point, if a suitable fluid-dynamic model for particle entrapment is developed.

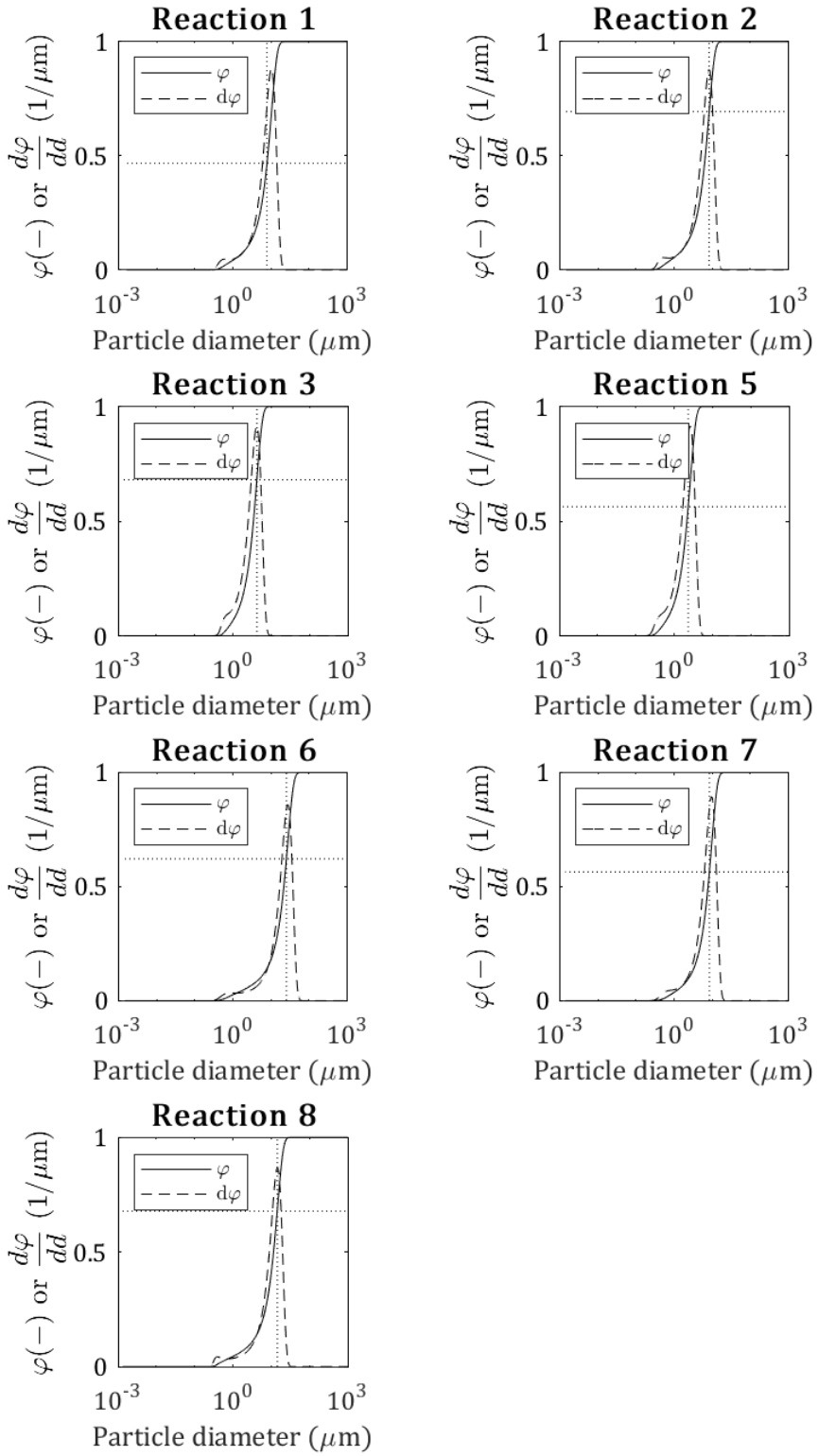

Figure 7. Cumulative frequency (in particle volume) and its derivative for each reaction. Horizontal dotted lines are drawn at Φ, and the vertical ones are plotted as a visual aid to show the point at which φ = Φ.

5. Conclusions

In this work, a population balance model was developed in an attempt to reproduce the phase inversion behavior of the reacting system during the bulk polymerization of HIPS, for a given set of reaction conditions. The evolution of the dispersed phase (PS-rich) along the reaction was modeled following a heterogeneous polymerization model that accounts for the monomer partition between both phases. This effect forces the dispersed phase to grow along the reaction, especially before the PI point. Coalescence and break-up of vitreous particles were computed with expressions available in literature, and particle size distributions were predicted for each reaction condition.

Results show that predictions are in very good agreement with measured particle sizes. With the adjusted model, the most popular criterion for phase inversion – the coalescence *vs* breakage imbalance – was assessed. The analysis shows that the coalescence-to-breakage ratio never spikes at any point during the polymerizations. After careful physical analysis, it is concluded that (at least in this system) it is likely that this feature is never observed, as the inversion process does not occur in an accelerated, "instantaneous" way. Rather, it is the result of a co-continuous transition that may last several minutes. In order to test the physical reliability of the model, cumulative frequency curves were produced and compared to the expected behaviors around the inversion points. These are shown to be in very good agreement with what would be anticipated at such points.

The future goal of this work is to identify a clear phase inversion criterion that can apply in the polymerization of HIPS and to develop a comprehensive mathematical model that is able to predict both its occurrence and the morphology therein developed.

6. Nomenclature

Symbol	Reference	Unit
β	Daughter particle size distribution	--
γ	Interfacial tension	N/m
$\dot{\gamma}$	Shear rate	1/s
δ	Dirac's delta function	--
ε	Turbulent energy dissipation rate	m^2/s^3
ζ	Grafting efficiency	--
η	Apparent viscosity	cP
λ_c	Coalescence efficiency	--
ρ	Density	kg/m^3
σ	Surface tension	N/m
ϕ	Phase volume fraction	--
Φ	Fraction of vitreous phase that participates in the inversion process	--
φ	Cumulative frequency (in particle volume)	--
χ	Flory-Huggins parameter	--
ω	Fractional break-up or coalescence frequency	
Ω	Total particle break-up or coalescence frequency	
d	Particle diameter	μm
D	Diameter	
f	Number density function	$1/m^3$
m	Mass	kg
M_w	Weight-average molecular weight	
n	Stirring speed	1/s
$\widehat{N}$	Number of dispersed particles per unit volume	$1/m^3$
Rp	Polymerization rate	mol/s
T	Temperature	K
V	Volume	m^3
w	Weight fraction	
x	PS conversion	--
z	Polymerization degree	--
Subscripts		
b	Breakage	
c	Coalescence / Continuous phase	
cd	Colliding drops	
d	Dispersed phase	
oc	Occluded vitreous phase	
r	Rubber-rich phase	
v	Vitreous phase	

v,c	Vitreous continuous phase
I	Impeller
PI	Phase inversion point
PS,v	Polystyrene in vitreous phase
PS	Polystyrene
PB	Polybutadiene
St	Styrene
T	Total / Tank

7. Acknowledgments

The authors are grateful to Instituto Tecnológico de Buenos Aires (ITBA) for their financial support through grant ITBACyT 45/2020 and to CONICET for the postdoctoral fellowship granted to Dr. Maffi.

8. References

[1] C. Luciani, D.A. Estenoz, G. Morales, G.R. Meira, High impact polystyrene (HIPS). Predicting its molecular, morphological and mechanical properties, in: Proc. CONAMET/SAM Congr., La Serena, Chile, 2004.

[2] Y. Okamoto, H. Miyagi, M. Kakugo, K. Takahashi, Impact improvement mechanism of HIPS with bimodal distribution of rubber particle size, Macromolecules. 24 (1991) 5639–5644.

[3] M.R. Rivera, R. Herrera, L. Ríos, Structure and properties of model polybutadienes and HIPS: effect of rubber microstructure on HIPS dynamic mechanical properties, J. Elastomers Plast. 38 (2006) 133–146. https://doi.org/10.1177/0095244306057255.

[4] R.L. Kruse, Styrene-polymer interaction parameters in high impact polystyrene, in: Copolym. Polyblends Compos. A Symp., American Chemical Society, Washington D. C., 1975: pp. 141–147.

[5] N. Casis, C. V. Luciani, D.A. Estenoz, M. Martinelli, M. Strumia, G.R. Meira, Partition of tert-dodecyl mercaptan in systems containing styrene, polystyrene, and polybutadiene. Its effect on the macromolecular characteristics of high-impact poly styrene, E-Polymers. 85 (2007) 5–10.

[6] F. Soriano-Corral, G. Morales, P. Acuña, E. Diaz Barriga, B. Arellano, C. Vargas, O. De La Paz, Synthesis and Characterization of High Impact Polystyrene from a Heterogeneous Styrene-Rubber-Polystyrene Solution : Influence of PS Concentration on the Phase Inversion , Morphology and Impact Strength, Macromol. Symp. 325–326 (2013) 177–183. https://doi.org/10.1002/masy.201200059.

[7] G.F. Freeguard, M. Karmarkar, The production of rubber-modified polystyrene. I. Rheological behavior of the polymerizing system, J. Appl. Polym. Sci. 15 (1971) 1649–1655. https://doi.org/10.1002/app.1971.070150708.

[8] Z. Song, H. Yuan, Z. Pen, Studies on the rheological behavior of high-impact polystyrene prepolymerizing systems, J. Appl. Polym. Sci. 32 (1986) 3349–3369. https://doi.org/10.1002/app.1986.070320201.

[9] R. Díaz de León, G. Morales, P. Acuña, F. Soriano, Phenomenon of Phase Inversion in High Impact Polystyrene: Physico-Chemical, Rheological and Morphological Study in the Presence of Chain Transfer Agent and Using Different Tapered Block Copolymers as the Precursor Rubber, Polym. Eng. Sci. 50 (2010) 373–383. https://doi.org/10.1002/pen.

[10] G.M. Jordhamo, J. a. Manson, L.H. Sperling, Phase Continuity and Inversion in Polymer Blends and Simultaneous Interpenetrating Networks, Polym. Eng. Sci. 26 (1986) 517–524. https://doi.org/10.1002/pen.760260802.

[11] G. Riess, Morphology control in polymeric multiphase systems with block copolymers and structured latexes, Makromol. Chemie. Macromol. Symp. 69 (1993) 125–131. https://doi.org/10.1002/masy.19930690113.

[12] M. Fischer, G.P. Hellmann, On the Evolution of Phase Patterns during the High-Impact-Modified Polystyrene Process, Macromolecules. 29 (1996) 2498–2509. https://doi.org/10.1021/ma950779a.

[13] A.A. Alfarraj, E.B. Nauman, Reactive phase separation : Prediction of an occlusion morphology, Polymer (Guildf). 49 (2008) 339–344. https://doi.org/10.1016/j.polymer.2007.09.035.

[14] N. Mekhilef, H. Verhoogt, Phase inversion and dual-phase continuity in polymer blends: Theoretical predictions and experimental results, Polymer (Guildf). 37 (1996) 4069–4077. https://doi.org/10.1016/0032-3861(96)00254-6.

[15] T.H. Chen, A.C. Su, Morphology of poly(p-phenylene sulfide)polyethylene blends, Polymer (Guildf). 34 (1993) 4826–4831. https://doi.org/10.1016/0032-3861(93)90004-T.

[16] J.M. Maffi, G.R. Meira, D.A. Estenoz, Mechanisms and conditions that affect phase inversion processes. A review, Can. J. Chem. Eng. 99 (2021) 178–208.

[17] J. Alvarez, J. Alvarez, M. Hernández, A population balance approach for the description of particle size distribution in suspension polymerization reactors, Chem. Eng. Sci. 49 (1994) 99–113. https://doi.org/10.1016/0009-2509(94)85037-2.

[18] L.M. Oshinowo, C.G. Quintero, R.D. Vilagines, CFD and Population Balance Modeling of Crude Oil Emulsions in Batch Gravity Separation—Comparison to Ultrasound Experiments, J. Dispers. Sci. Technol. 37 (2016) 665–675. https://doi.org/10.1080/01932691.2015.1054508.

[19] D. Li, A. Buffo, W. Podgórska, D.L. Marchisio, Z. Gao, Investigation of droplet breakup in liquid–liquid dispersions by CFD–PBM simulations: The influence of the

surfactant type, Chinese J. Chem. Eng. 25 (2017) 1369–1380. https://doi.org/10.1016/j.cjche.2017.01.014.

[20] S. Aryafar, N. Sheibat-Othman, T.F.L. McKenna, Coupling of CFD Simulations and Population Balance Modeling to Predict Brownian Coagulation in an Emulsion Polymerization Reactor, Macromol. React. Eng. 11 (2017) 1–17. https://doi.org/10.1002/mren.201600054.

[21] L. Xie, Q. Liu, Z.H. Luo, A multiscale CFD-PBM coupled model for the kinetics and liquid–liquid dispersion behavior in a suspension polymerization stirred tank, Chem. Eng. Res. Des. 130 (2018) 1–17. https://doi.org/10.1016/j.cherd.2017.11.045.

[22] B. Hu, O.K. Matar, G.F. Hewitt, P. Angeli, Population balance modelling of phase inversion in liquid–liquid pipeline flows, Chem. Eng. Sci. 61 (2006) 4994–4997. https://doi.org/10.1016/j.ces.2006.03.053.

[23] G.P. Leal, J.M. Asua, Evolution of the morphology of HIPS particles, Polymer (Guildf). 50 (2009) 68–76. https://doi.org/10.1016/j.polymer.2008.10.035.

[24] J.M. Maffi, N. Casis, P. Acuña, G. Morales, D.A. Estenoz, Mechanisms and Conditions that Affect Phase Inversion Processes. The Case of High-Impact Polystyrene, Polym. Eng. Sci. 60 (2020) 491–502. https://doi.org/10.1002/pen.25304.

[25] N. Casis, D. Estenoz, L. Gugliotta, H. Oliva, G. Meira, Heterogeneous Bulk Polymerization of Styrene in the Presence of Polybutadiene: Calculation of the macromolecular structure, J. Appl. Polym. Sci. 99 (2006) 3023–3039. https://doi.org/10.1002/app.22902.

[26] A.S. Kabalnov, A. V. Pertzov, E.D. Shchukin, Ostwald ripening in emulsions. I. Direct observations of Ostwald ripening in emulsions, J. Colloid Interface Sci. 118 (1987) 590–597. https://doi.org/10.1016/0021-9797(87)90492-9.

[27] J. Rauch, W. Köhler, Diffusion and Thermal Diffusion of Semidilute to Concentrated Solutions of Polystyrene in Toluene in the Vicinity of the Glass Transition, Phys. Rev. Lett. 88 (2002) 4. https://doi.org/10.1103/PhysRevLett.88.185901.

[28] Y. Liao, D. Lucas, A literature review of theoretical models for drop and bubble breakup in turbulent dispersions, Chem. Eng. Sci. 64 (2009) 3389–3406. https://doi.org/10.1016/j.ces.2009.04.026.

[29] Y. Liao, D. Lucas, A literature review on mechanisms and models for the coalescence process of fluid particles, Chem. Eng. Sci. 65 (2010) 2851–2864. https://doi.org/10.1016/j.ces.2010.02.020.

[30] D.Y.C. Chan, E. Klaseboer, R. Manica, Film drainage and coalescence between deformable drops and bubbles, Soft Matter. 7 (2011) 2235–2264. https://doi.org/10.1039/C0SM00812E.

[31] S.P. Lyu, F.S. Bates, C.W. Macosko, Coalescence in polymer blends during shearing, AIChE J. 46 (2000) 229–238. https://doi.org/10.1002/aic.690460203.

[32] S. Lyu, F.S. Bates, C.W. Macosko, Modeling of Coalescence in Polymer Blends, AIChE J. 48 (2002) 7–14. https://doi.org/10.1002/aic.690480103.

[33] U. Sundararaj, C.W. Macosko, Drop Breakup and Coalescence in Polymer Blends: The Effects of Concentration and Compatibilization, Macromolecules. 28 (1995) 2647–2657. https://doi.org/10.1021/ma00112a009.

[34] V. Alopaeus, J. Koskinen, K.I. Keskinen, J. Majander, Simulation of the population balances for liquid-liquid systems in a nonideal stirred tank. Part 2-parameter fitting and the use of the multiblock model for dense dispersions, Chem. Eng. Sci. 57 (2002) 1815–1825. https://doi.org/10.1016/S0009-2509(02)00067-2.

[35] M.A.A. Hsia, L.L. Tavlarides, Simulation analysis of drop breakage, coalescence and micromixing in liquid-liquid stirred tanks, Chem. Eng. J. 26 (1983) 189–199. https://doi.org/10.1016/0300-9467(83)80014-8.

[36] B. Hu, P. Angeli, O.K. Matar, G.F. Hewitt, Prediction of phase inversion in agitated vessels using a two-region model, Chem. Eng. Sci. 60 (2005) 3487–3495. https://doi.org/10.1016/j.ces.2005.02.002.

[37] H. Sovová, Breakage and coalescence of drops in a batch stirred vessel II - Comparison of model and experiments, Chem. Eng. Sci. 36 (1981) 1567–1573. https://doi.org/10.2307/3564503.

[38] Y. Song, S.M. Lambert, J.M. Prausnitz, Equation of state of mixtures of hard-sphere chains including copolymers, Macromolecules. 27 (1997).

[39] E. Jurado, V. Bravo, F. Camacho, J.M. Vicaria, A. Fernández-Arteaga, Estimation of the distribution of droplet size, interfacial area and volume in emulsions, Colloids Surfaces A Physicochem. Eng. Asp. 295 (2007) 91–98. https://doi.org/10.1016/j.colsurfa.2006.08.037.

[40] N. Nizamidin, U.P. Weerasooriya, G.A. Pope, Systematic Study of Heavy Oil Emulsion Properties Optimized with a New Chemical Formulation Approach: Particle Size Distribution, Energy and Fuels. 29 (2015) 7065–7079. https://doi.org/10.1021/acs.energyfuels.5b01818.

[41] J. Solsvik, P.J. Becker, N. Sheibat-Othman, H.A. Jakobsen, Population balance model: Breakage kernel parameter estimation to emulsification data, Can. J. Chem. Eng. 92 (2014) 1082–1099. https://doi.org/10.1002/cjce.21928.

[42] S. Kumar, D. Ramkrishna, On the solution of population balance equations by discretization - II. A moving pivot technique, Chem. Eng. Sci. 51 (1996) 1333–1342. https://doi.org/10.1016/0009-2509(95)00355-X.

[43] S. Kumar, D. Ramkrishna, On the solution of population balance equations by discretization - III. Nucleation, growth and aggregation of particles, Chem. Eng. Sci. 52 (1997) 4659–4679. https://doi.org/10.1016/S0009-2509(97)00307-2.

[44] A. Bakker, L. Gates, Properly Choose Mechanical Agitators for Viscous Liquids, Chem. Eng. Prog. 91 (1995) 25–34.

[45] D.Y. Kwok, A.W. Neumann, Contact angle measurement and contact angle interpretation, Adv. Colloid Interface Sci. 81 (1999) 167–249. https://doi.org/10.1016/S0001-8686(98)00087-6.

[46] J. Noolandi, K.M. Hong, Effect of Block Copolymers at a Demixed Homopolymer Interface, Macromolecules. 17 (1984) 1531–1537.

[47] P.C. Painter, M.M. Coleman, Fundamentals of Polymer Science, 1st ed., Technomic Publishing Co., Lancaster, 1997.

[48] J. Noolandi, K.M. Hong, Theory of block copolymer micelles in solution, Macromolecules. 16 (1983) 1443–1448.

[49] J. Noolandi, K.M. Hong, Interfacial Properties of Immiscible Homopolymer Blends in the Presence of Block Copolymers, Macromolecules. 1 (1982) 482–492.

[50] M.A. Cerpa-Gallegos, C.F. Jasso-Gastinel, V.A. Lara-Valencia, L.J. González-Ortiz, Improved methodology to measure surface tension and its application to polystyrene or poly(methyl methacrylate) in styrene solutions, Langmuir. 21 (2005) 7726–7732. https://doi.org/10.1021/la050095o.

[51] I. Prigogine, J. Marechal, The influence of differences in molecular size on the surface tension of solutions. IV., J. Colloid Sci. 7 (1952) 122–127.

[52] G.M. Kontogeorgis, S. Kiil, Introduction to Applied Colloid and Surface Chemistry, John Wiley & Sons, 2016.

[53] D.W.W. van Krevelen, K. te Nijenhuis, Properties of Polymers, 4th ed., Elsevier B.V., 2009. https://doi.org/10.1016/B978-0-444-82877-4.50021-4.

[54] A.W. Hui, A.E. Hamielec, Thermal Polymerization of Styrene at High Conversion and Temperatures. An Experimental Study, J. Appl. Polym. Sci. 16 (1972) 749–769. https://doi.org/10.1002/app.1972.070160319.

[55] R.P. Danner, M.S. High, Handbook of Polymer Solution Thermodynamics, American Institute of Chemical Engineers, New York, 1993. https://doi.org/10.1002/9780470938232.

[56] J. Ansorena, J.J. Iruin, G.M. Guzmán, Solvent influence on the viscosity-temperature relationship for dilute polybutadiene solutions, Eur. Polym. J. 16 (1980) 165–167.

[57] J.M. Maffi, Theoretical and Experimetnal Study on the Phase Inversion Process during the Bulk Synthesis of High Impact Polystyrene, Instituto Tecnológico de Buenos Aires, 2021.

[58] D. Kim, E.B. Nauman, Solution viscosity of polystyrene at conditions applicable to commercial manufacturing processes, J. Chem. Eng. Data. 37 (1992) 427–432.

[59] D.A. Estenoz, E. Valdez, H. Oliva, G.R. Meira, Bulk polymerization of styrene in presence of polybutadiene: Calculation of molecular macrostructure, J. Appl. Polym. Sci. 59 (1996) 861–885. https://doi.org/10.1002/(SICI)1097-4628(19960131)59:5<861::AID-APP12>3.3.CO;2-J.

[60] N. Friis, A.E. Hamielec, Gel-effect in emulsion polymerization of vinyl monomers, ACS Symp. Ser. 24 (1976) 82–91.

[61] F.R. Mayo, The Dimerization of Styrene, J. Am. Chem. Soc. 90 (1968) 1289–1295. https://doi.org/10.1021/ja01007a032.

[62] J.L. Ou, J.K. Yang, H. Chen, Styrene/potassium persulfate/water systems: Effects of hydrophilic comonomers and solvent additives on the nucleation mechanism and the particle size, Eur. Polym. J. 37 (2001) 789–799. https://doi.org/10.1016/S0014-3057(00)00175-0.

[63] E.R. Soulé, G.E. Eliçabe, J. Borrajo, R.J.J. Williams, Analysis of the phase separation induced by a free-radical polymerization in solutions of polyisobutylene in isobornyl methacrylate, Ind. Eng. Chem. Res. 46 (2007) 7535–7542. https://doi.org/10.1021/ie061567c.

[64] L.E. Redington, Diacyl peroxides as polymerization initiators: rate of polymerization of styrene in relation to rate of decomposition of four organic peroxides, J. Polym. Sci. 3 (1948) 503–517.

[65] F.M. Peng, M.C. Company, Polybutadiene Grafting and Crosslinking in High-Impact Polystyrene Bulk Thermal Process, 40 (1990) 1289–1302.

[66] M.S. Matheson, E.E. Auer, E.B. Bevilacqua, E.J. Hart, Rate Constants in Free Radical Polymerization. III. Styrene, J. Am. Chem. Soc. 73 (1951) 1700–1706.

[67] A.K. Chesters, The modelling of coalescence process in fluid-liquid dispersions: A Review of Current Understanding, Chem. Eng. Res. Des. 69 (1991) 259–270.

[68] F. Groeneweg, W.G.M. Agterof, P. Jaeger, J.J.M. Janssen, J.A. Wieringa, J.K. Klahn, On the Mechanism of the Inversion of Emulsions, Chem. Eng. Res. Des. 76 (1998) 55–63. https://doi.org/10.1205/026387698524596.

[69] K. Ioannou, O. Jorgen, P. Angeli, Phase inversion in dispersed liquid – liquid flows, Exp. Therm. Fluid Sci. 29 (2005) 331–339. https://doi.org/10.1016/j.expthermflusci.2004.05.003.

[70] F. Bouchama, G.A. Van Aken, A.J.E.E. Autin, G.J.M.M. Koper, On the mechanism of catastrophic phase inversion in emulsions, Colloids Surfaces A Physicochem. Eng. Asp. 231 (2003) 11–17. https://doi.org/10.1016/j.colsurfa.2003.08.011.

[71] C. Pierlot, J.F. Ontiveros, M. Royer, M. Catté, J.L. Salager, Emulsification of viscous alkyd resin by catastrophic phase inversion with nonionic surfactant, Colloids Surfaces A Physicochem. Eng. Asp. 536 (2018) 113–124. https://doi.org/10.1016/j.colsurfa.2017.07.030.

9. Appendix

9.1. Rubber-rich phase

Initiator

$$\frac{d}{dt}([I_2]_r V_r) = -k_d[I_2]_r V_r \quad \text{(A. 1)}$$

Monomer

$$\frac{d}{dt}(M_{St}[St]_r V_r) = -k_p[St]_r([S^\bullet]_r + [P^\bullet])M_{St}V_r - \dot{F} \quad \text{(A. 2)}$$

Ungrafted butadiene units

$$\frac{d}{dt}([B]V_r) = -\{k_{i2}[I^\bullet]_r + k_{fG}([S^\bullet]_r + [P^\bullet])\}[B]V_r + k_{fM}[St]_r[P_0^\bullet]V_r \quad \text{(A. 3)}$$

Radical species

$$\frac{d}{dt}([I^\bullet]_r V_r) = 2fk_d[I_2]_r - k_{i1}[St]_r[I^\bullet]_r V_r - \frac{\dot{F}}{\rho_{St}}[I^\bullet]_r \quad \text{(A. 4)}$$

$$\begin{aligned}\frac{d}{dt}([S_1^\bullet]_r V_r) = \{&k_{i1}[St]_r[I^\bullet]_r + 2k_{i0}[St]_r{}^3 - k_p[St]_r[S_1^\bullet]_r \\ &+ k_{fM}[St]_r([S^\bullet]_r + [P^\bullet] + [P_0^\bullet])\}V_r \\ &- \{k_{fG}[B] + k_{tcr}([S^\bullet]_r + [P^\bullet] + [P_0^\bullet])\}[S_1^\bullet]_r V_r - \frac{\dot{F}}{\rho_{St}}[S_1^\bullet]_r\end{aligned} \quad \text{(A. 5)}$$

$$\begin{aligned}\frac{d}{dt}([S_n^\bullet]_r V_r) = &k_p[St]_r[S_{n-1}^\bullet]_r V_r \\ &- \{k_p[St]_r + k_{fM}[St]_r + k_{fG}[B] \\ &+ k_{tcr}([S^\bullet]_r + [P^\bullet] + [P_0^\bullet])\}[S_n^\bullet]_r V_r - \frac{\dot{F}}{\rho_{St}}[S_n^\bullet]_r\end{aligned} \quad \text{(A. 6)}$$

for n>1

$$\frac{d}{dt}([P_0^\bullet]V_r) = \left\{k_{i2}[I^\bullet]_r + k_{fG}([S^\bullet]_r + [P^\bullet])\right\}[B]V_r - \left\{k_{i3}[St]_r + k_{fM}[St]_r + k_{tcr}([S^\bullet]_r + [P^\bullet] + [P_0^\bullet])\right\}[P_0^\bullet]V_r \quad \text{(A. 7)}$$

$$\frac{d}{dt}([P_1^\bullet]V_r) = k_{i3}[St]_r[P_0^\bullet]V_r - \left\{k_p[St]_r + k_{fM}[St]_r + k_{fG}[B] + k_{tcr}([S^\bullet]_r + [P^\bullet] + [P_0^\bullet])\right\}[P_1^\bullet]_r V_r \quad \text{(A. 8)}$$

$$\frac{d}{dt}([P_n^\bullet]V_r) = k_p[St]_r[P_{n-1}^\bullet]_r V_r - \left\{k_p[St]_r + k_{fM}[St]_r + k_{fG}[B] + k_{tcr}([S^\bullet]_r + [P^\bullet] + [P_0^\bullet])\right\}[P_n^\bullet]_r V_r \quad \text{(A. 9)}$$

for n>1

Equations (A. 5) and (A. 6) may be combined to obtain the total balance for St radicals in the rubber-rich phase, and adding (A. 7) to (A. 9) yields the balance for all P radicals.

Phase volume

$$\frac{d}{dt}(V_r) = \frac{-k_p[St]_r([S^\bullet]_r + [P^\bullet])V_r M_{St} - \dot{F}}{\rho_{St}} \quad \text{(A. 10)}$$

9.2. Vitreous phase

Initiator

$$\frac{d}{dt}([I_2]_v V_v) = -k_d[I_2]_v V_v \quad \text{(A. 11)}$$

Monomer

$$\frac{d}{dt}(M_{St}[St]_v V_v) = -k_p[St]_v[S^\bullet]_v M_{St} V_v + \dot{F} \quad \text{(A. 12)}$$

Radical species

$$\frac{d}{dt}([I^\bullet]_v V_v) = 2fk_d[I_2]_v V_v - k_{i1}[St]_v[S^\bullet]_v[I^\bullet]_v V_v + \frac{\dot{F}}{\rho_{St}}[I^\bullet]_r \quad \text{(A. 13)}$$

$$\frac{d}{dt}([S_1^\bullet]_v V_v) = \{k_{i1}[St]_v[I^\bullet]_v + 2k_{i0}[St]_v{}^3 - k_p[St]_v[S_1^\bullet]_v + k_{fM}[St]_v[S^\bullet]_v - k_{tcv}[S^\bullet]_v[S_1^\bullet]_v\}V_v - \frac{\dot{F}}{\rho_{St}}[S_1^\bullet]_r \quad \text{(A. 14)}$$

$$\frac{d}{dt}([S_n^\bullet]_v V_v) = k_p[St]_v[S_{n-1}^\bullet]_v V_v - \{k_p[St]_v + k_{fM}[St]_v + k_{tcv}[S^\bullet]_v\}[S_n^\bullet]_v V_v - \frac{\dot{F}}{\rho_{St}}[S_n^\bullet]_r \quad \text{(A. 15)}$$

for n>1

Equations XY may be combined to obtain the total balance for St radicals in the rubber-rich phase, and adding YZ yields the balance for all P radicals.

Phase volume

$$\frac{d}{dt}(V_v) = \frac{-k_p[St]_v[S^\bullet]_v V_v M_{St} + \dot{F}}{\rho_{St}} + \frac{k_p[St]_v[S^\bullet]_v V_v M_{St}}{\rho_{PS}} \quad \text{(A. 16)}$$

9.3. Chain length distribution of PS

The number chain length distribution (NCLD) is calculated by computing the mass balance for each PS species in each phase, following Casis et al. [25].